Biophysical Journal, Volume 97

Supporting Material

DySCo: Quantitating associations of membrane proteins using two-color single-molecule tracking

Paul D Dunne, Ricardo A Fernandes, James McColl, Ji Won Yoon, John R James, Simon J Davis, and David Klenerman

Supporting information:

DySCo: Quantitating associations of membrane proteins using two-color single-molecule tracking

Paul D Dunne,[†||] Ricardo A Fernandes,[‡||] James McColl,[†||] Ji Won Yoon,[§] John R James,[‡¶] Simon J Davis,*[‡] David Klenerman*[†]

[†]Department of Chemistry, University of Cambridge, Lensfield Road, Cambridge CB2 1EW, UK; [‡]Nuffield Department of Clinical Medicine and Medical Research Council Human Immunology Unit and The Weatherall Institute of Molecular Medicine, University of Oxford, John Radcliffe Hospital, Headington, Oxford OX3 9DS, UK; [§]Department of Engineering Science, University of Oxford, Parks Road, Oxford, OX1 3PJ, UK; [¶]Present address: Department of Cellular and Molecular Pharmacology, University of California at San Francisco, San Francisco, CA 94158. [||]These authors contributed equally to this work.

*Correspondence to: David Klenerman, e-mail: dk10012@cam.ac.uk or Simon Davis, email: simon.davis@ndm.ox.ac.uk

SUPPORTING MATERIALS AND METHODS

- Vector Constructs
- Cell Culture and Lentivirus Infections
- Latrunculin Treatment of Cells
- Sample Preparation for Microscopy
- TIRFM Experimental Setup
- Bayesian Tracking Approach
- MSD Calculation and Positional Accuracy
- Colocalization Distance Criterion
- Calculation of % Coincidence

SUPPORTING RESULTS

- Protein Expression at the Cell Surface
- Triggering Assay
- Diffusion Coefficients

SUPPORTING DISCUSSION

- Fluorophore Stability

SUPPORTING MATERIALS AND METHODS

Vector Constructs

The sequences of all genes were amplified using PCR from cDNA, IMAGE sequences or previously cloned vectors. For CD28, CD86 and TCRβ the stop codons were mutated for an appropriate restriction enzyme and the genes then inserted, in frame at the N-Terminus of 3x Citrine or 3x mCherry proteins. All genes were sequenced to confirm both the reading frame and integrity. We modified the SFFV promoter on the pHR lentiviral vector (kindly provided by Yasuhiro Ikeda, Mary Collins lab, UCL) to an ecdysone-inducible promoter, producing the pHR Inducible vector, pHRI. In the absence of ecdysone or any other analogue the genes encoded on pHRI vector are transcribed at low levels.

Cell Culture and Lentivirus Infections

Lentivirus infections were used to generate stably transfected cell lines expressing the desired genes. HEK293T cells, grown in DMEM supplemented with 10% FCS, 1% HEPES buffer, 1% sodium pyruvate and 1% antibiotics, were plated in six well plates, $6x10^5$ cells/plate (all reagents from Sigma Aldrich, Dorset, UK). After 24 hours cells were transfected with equal amounts of pHRI vector (including the gene of interest), p8.91 and pMDG (kindly provided by Yasuhiro Ikeda, Mary Collins lab, UCL) using Genejuice (Novagen Merck, Hull, UK) (1). 48 hours later the supernatant from two six well plates was removed and added to $1x10^6$ Jurkat (for CD86) or J.RT3 cells (for CD28 and TCRβ since these are $CD28^-$ and $TCR\beta^-$). These cells were grown in phenol red free RPMI supplemented with 10% FCS, 1% HEPES buffer, 1% sodium pyruvate and 1% antibiotics. Cells were analysed using FACS after 5 days of lentiviral infection to confirm expression of the desired proteins.

Latrunculin Treatment of Cells

Latrunculin B (Biomol International, Exeter, UK) was dissolved in dimethyl sulfoxide (DMSO from Alfa Aesar, Heysham, UK) to a concentration of 2.5 mM. Cells were incubated at 37°C in supplemented RPMI media containing 2.5 μM latrunculin B for 20 minutes to disrupt actin formation. Following re-suspension in phosphate buffered saline (PBS; 150 mM NaCl, 10mM $HNaPO_4$ (Sigma Aldrich Dorset, UK) in ultrapure water (MilliQ 18.2 MΩ), pH 7.2) the cells were imaged using the same protocol as for untreated cells.

Sample Preparation for Microscopy

Microscope coverslips were cleaned for 1 hour in Piranha solution (3:1 sulfuric acid:hydrogen peroxide) and thoroughly rinsed with ultrapure water (MilliQ 18.2 MΩ) before incubating with 100 μl of 20 μg/ml donkey anti-mouse, non-specific IgG antibody (Jackson Immunoresearch Europe, UK) at 37°C for 1 hour. Cells were centrifuged at 600 × *g* for 2 minutes and the supernatant removed, before resuspending in 37°C PBS solution for imaging. Slides were rinsed again to remove non-adsorbed antibody and transferred to a heated microscope stage. Cells were added and allowed to settle for 5 minutes and imaged within the subsequent 15 minutes.

TIRFM Experimental Setup

Imaging was performed using total internal reflection fluorescence microscopy (TIRFM), restricting detectable fluorescence signal to within ~100 nm from the sample slide (2). Briefly, the output from a dual line Kr/Ar laser operating at 488 and 568 nm (353-LDL-840-240, Melles Griot) was directed down the edge of a 1.45 NA TIRF objective (60x Plan Apo TIRF, NA 1.45, Nikon) mounted on a Nikon TE2000-U microscope. Fluorescence collected by the same objective was separated from the returning TIR beam by a dichroic (490575DBDR, Omega Optical), split into yellow and red components (585 DXLR, Omega Optical, Brattleboro, VT) and filtered using Dual-View™ (Optical Insights) mounted filters. The images were simultaneously recorded on an EMCCD (Cascade II: 512 Princeton instruments, MA) whereby the EMCCD was split so that each color was recorded on one half of the EMCCD, operating at minus 70°C. Data were acquired at 17.8 frames s^{-1} using IPlab 4.0.2 software (BDBiosciences, Rockville, MD).

The 488 nm beam was attenuated by 64 % using filters (Comar, Cambridge, UK). The laser power used for taking measurements being 1.2 mW for the 568 channel and 0.35 mW for the 488 (as measured by epifluorescence at the sample plane) over an area of ~45 μm diameter. Images were taken for 30 frames and data only captured during the first 20 minutes after cells began to attach to the surface.

To achieve good image registration, a grid consisting of regularly spaced ion-beam etched holes in gold-on-glass was utilized. Dual-View™ optics were adjusted so as to maximize the overlap between red and green images of the grid under white-light illumination, resulting in measured image registrations in the range of ~75 nm.

Bayesian Tracking Approach

Tracking was carried out using custom software implemented in MATLAB (The MathWorks, Natick, MA). The Bayesian based algorithm is an extension of work by Oh *et al* (3) and similar to our published Bayesian method (4).

After detecting centroid positions of potential targets above a user defined threshold (5) (five standard deviations above the image mean pixel count for this work), the program links spots using a Markov Chain Monte Carlo (MCMC) algorithm programmed within a Bayesian framework (for details of Bayesian formulation see Yoon *et al.* (4)). Detected spots are initially linked at random over the entire image sequence and this configuration is assigned a possible likelihood according to its statistical fit to Brownian behavior. The program then iterates the configuration, with several possible outcomes at each iteration:

- Birth (new track is proposed)
- Death (track is removed)
- Split (track splits into smaller tracks)
- Merge (smaller tracks are merged)
- Update (track configuration is altered)
- Increase (track increases in length)
- Decrease (track decreases in length).

With increasing iterations the program approaches the most likely configuration, which may not always give the same result as those from traditional deterministic tracking (as found for our previous algorithm (4)). Very few initial parameters are specified by the user- thus the contribution of error introduced by poor parameter initialization is minimized.

This method differs from our published method (4) in two important ways that decrease the computational complexity significantly. In the initial implementation, particle detection was incorporated into the Bayesian framework, but for the analysis in this work we identify objects as peaks above a user defined threshold, using an established method (5). This means we need not consider every pixel in the image when it comes to the tracking step. The tracking for our previous implementation used a Sequential Monte Carlo (SMC) algorithm, with tracks being updated at each frame based on their previous history. That is to say, after the n^{th} frame is processed, the result is inputted into the calculation for the $(n+1)^{th}$ frame, and is not considered again. For this paper, tracking is carried out using a MCMC method, whereby the whole video sequence is considered for each iteration. This method has the advantage of being far less sensitive to the initial configuration. Further details will be included in a future publication (6).

The software can be made freely available upon request.

MSD Calculation and Positional Accuracy

We performed mean-square displacement (MSD) calculations on the data and fitted the first three points of the MSD curve to a linear equation,

$$MSD = 4Dt + A_0 \tag{1}$$

where D is the diffusion coefficient. The median and upper and lower quartiles are chosen to represent the overall distribution of D and A_0 for this work as the diffusion coefficients and A_0 have skewed distributions.

To estimate the inherent uncertainty, σ, in the assignment of particle positions, we use (7),

$$A_0 = 2\sigma^2 . \tag{2}$$

The mean positional accuracy across the six different datasets was found to be 67.3 ± 5.4 nm for the yellow channel, and 75.8 ± 3.2 nm for the red.

Colocalization Distance Criterion

We obtain the colocalization criterion from the root mean-square (RMS) deviations in the positional accuracies for yellow and red molecules using,

$$\sigma_t = (\sigma_{yellow}{}^2 + \sigma_{red}{}^2)^{1/2} \quad . \tag{3}$$

Using equation 3 with our positional accuracies calculated above gives a value of 101.4 nm. Hence, in order to obtain a 90% probability of colocalization the distance threshold is $1.65\sigma_{t,}$ corresponding to 167.3 nm (8). Adding the value for our image registration accuracy (see TIRFM Experimental Setup section above), gives a colocalization distance value of 242.3 nm. For this work we chose the colocalization distance of 300 nm, to minimise the chance of missing associated molecules.

Calculation of % Coincidence

After tracks were identified, we examined association by applying a nearest-neighbor distance approach (8,9). Distances between red and yellow tracks were calculated for each video frame, and a track determined as associated if it remained within the 300 nm colocalization distance for 3 or more frames. The overall coincidence is taken to be,

$$\%Coincidence = 100 \times \frac{number\ of\ colocalized\ tracks\ in\ red\ channel}{total\ number\ of\ tracks\ in\ red\ channel}, \quad (4)$$

with the red channel chosen due to the lower detection efficiency of events. The coincidence is calculated for each video and the overall coincidence for an experiment is taken as the mean across individual files.

To examine the contribution of chance coincidence, we repeated the colocalization analysis for all combinations of non-coupled red and yellow file pairs. The results of this analysis are present in Table S1.

Table S1: Red : yellow track colocalization. % coincident tracks for matched and shuffled files were determined for red and yellow tracks which remained within 300nm for at least three frames, errors are SEM. Subscript 'lat' denotes cells which were pre-treated with 2.5 μM latrunculin, a cytoskeletal disrupting molecule. "Blank" cells are Jurkat cells which do not express any fluorescent protein-tagged molecules.

	Cells	Tracks			Coincidence	
		Yellow	Red	% red tracks relative to yellow	Matched	Shuffled
CD28	25	434	269	62	22.7 ± 5.9	1.2 ± 0.3
CD86	27	332	257	77	10.2 ± 3.0	0.6 ± 0.1
TCR	23	242	177	73	4.8 ± 2.3	0.3 ± 0.1
$CD28_{lat}$	13	126	96	76	22.6 ± 7.6	0.7 ± 0.3
$CD86_{lat}$	16	143	124	87	3.3 ± 1.5	0.6 ± 0.2
TCR_{lat}	15	107	92	86	2.3 ± 1.2	0.4 ± 0.2
Blank cells	15	23	21	91	3.3 ± 3.2	-

To test how the distance threshold affected our results, the analysis was carried out at a range of distances, with the same overall trend observed above 200 nm (Figure S1). It seems that the detected coincidence observed for molecules remaining colocalized for 3 or more frames at a distance threshold of 100 nm is negligible, which is not surprising since this is a comparable length-scale to our positional accuracy in each color channel.

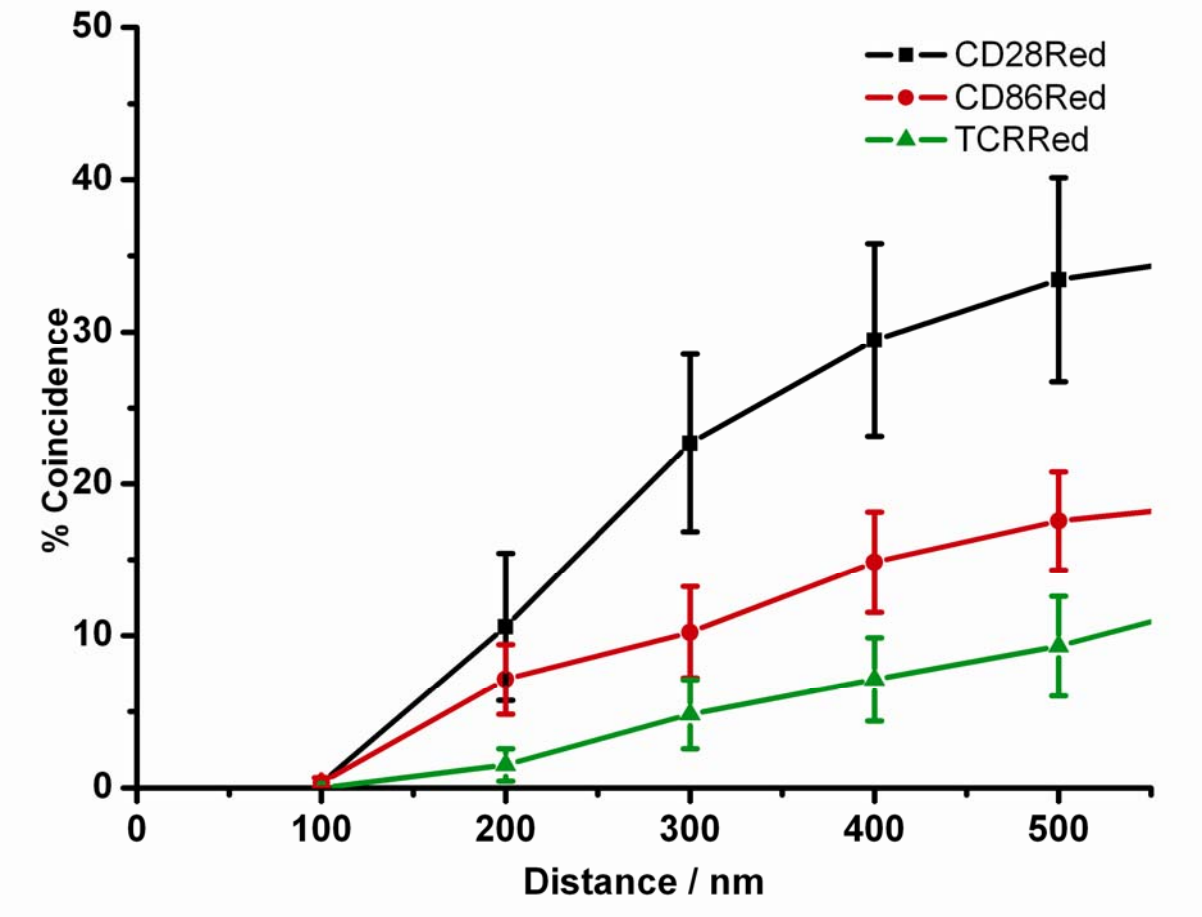

Figure S1: Coincidence dependence on varying distance (100-500 nm). Red and yellow coincidences were calculated at each distance. From this data we conclude that the observed behavior is not specific to a 300 nm colocalization distance. Errors are S.E.M.

SUPPORTING RESULTS

Protein Expression at the Cell Surface

Protein expression levels were quantitated using FACS in conjunction with QuantiBrite PE beads (Becton Dickinson, Oxford, United Kingdom), labeled with known levels of fluorescent R-phycoerythrin (PE) to calibrate the measured fluorescence of cell-bound PE-labeled antibodies to antigen density, as described in our previous work (10). The fluorescence values of the Quantibrite PE beads were acquired on a Cyan ADP flow cytometer in the FL2 channel, which were then used to construct a calibration curve that linearly related the number of PE molecules to the level of fluorescence. J.RT3 $CD86_{3xCitrine}$ and J.RT3 $CD28_{3xCitrine}$ (Citrine and mCherry kindly provided by Roger Y. Tsien) cells were incubated with either anti-CD86 (BU63) or anti-CD28 (7.3B6) PE-conjugated antibodies at 100 μg/ml for 60 min on ice. This ensured saturation of antigen sites and predominantly monovalent antibody binding. The measured PE fluorescence was then converted to the number of PE molecules per cell. Assuming univalent binding and 1:1 antibody:PE labelling (which is invariably the case) the number of PE molecules can be equated to antigen density. For the molecules in this study, the values are presented below (Table S2):

Table S2: Number of proteins on the T-cell surface

	Jurkat	J.RT3
Wild type	260	257
Isotype Control	438	256
J.RT3 $CD86_{3citrine}$	2109	-
J.RT3 $CD28_{3citrine}$	-	3467

Triggering Assay

To ensure that the presence of tandem cytocellular fluorescent proteins did not interfere with TCR function, we tested triggering using a modified NFAT assay (11). Briefly, following TCR signalling, Nuclear factor of activated T-cell (NFAT) transcription factors translocate from the cytosol to the nucleus. Here they initiate transcription of genes regulated by the NFAT promoter. T-cells were engineered to include a gene encoding *Renilla Luciferase* downstream of the NFAT promoter. Hence the level of cell activation could be probed by measuring *Renilla Luciferase* bioluminescence after adding coelentarazine h (Lux Biotechnology, Edinburgh, UK).

As expected, our $TCR\beta^-$ J.RT3 control cells showed an OKT3/OX7 ratio very close to 1, indicating zero activation (Figure S2). With expression of $TCR\beta_{TM}$ (native protein, no mCherry or Citrine) there was an increase in OKT3/OX7 and this was maintained for $TCR_{3xCitrine}$ and $TCR_{3xmCherry}$. The values are low and this is to be expected as we used the pHRI vector. Increasing the levels of TCR by expressing the protein using a pHR vector gave

an increase in the overall magnitude of the activation level, whilst the trend remained the same. As a comparison, Jurkats expressing around 10000 CD3ε on their surface were found to give an OKT3/OX7 ratio of 2.13, therefore the values for the pHRI cells suggest a good level of stimulation.

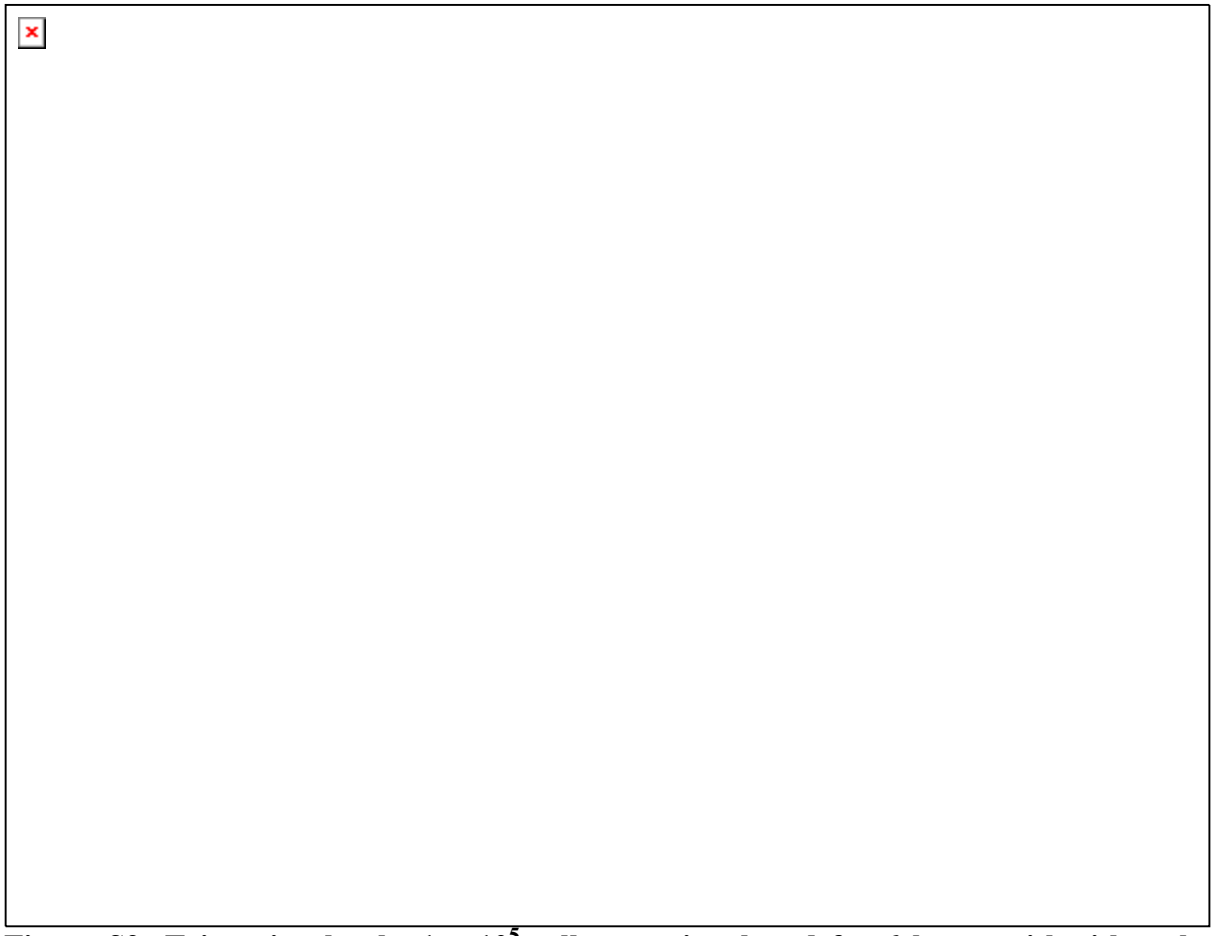

Figure S2: Triggering levels. 1 x 10^5 cells were incubated for 6 hours with either the triggering anti-CD3ε (OKT3) or non-triggering anti-Thy1 (OX7) soluble antibodies at 5 µg/ml. Bioluminescence was measured upon addition of 1 µg/ml coelentarazine and the data represented as a ratio of Renilla Luciferase activity in response to OKT3 and OX7 antibodies. Solid bar is result for wild type Jurkat cells and line-filled bars are for J.RT3 cells.

Diffusion Coefficients

Diffusion coefficients recovered were similar to those obtained by Fluorescence Correlation Spectroscopy (FCS) in a previous study (10) (Table S4), although the cell line and proteins differ slightly between these studies (Table S3). From this data it is clear that treating the cells with latrunculin leads to an increase in the rate of diffusion for CD86 and TCR, but decreases the median rate of diffusion for CD28. In conjunction with the colocalization measurements presented in Table S2, these data show that the behavior of TCR and CD86 upon latrunculin treatment differ to that observed for CD28, perhaps suggesting differences in the organization of these molecules at the cell surface.

Table S3: Diffusion coefficients for transgenically labeled proteins

		Median ($\mu m^2 s^{-1}$)	Upper Quartile ($\mu m^2 s^{-1}$)	Lower Quartile ($\mu m^2 s^{-1}$)	Number of tracks
CD28	Yellow	0.117	0.285	0.033	457
	Red	0.102	0.268	0.021	278
CD86	Yellow	0.073	0.225	0.017	328
	Red	0.109	0.323	0.017	267
TCR	Yellow	0.078	0.240	0.025	231
	Red	0.093	0.311	0.004	181
$CD28_{lat}$*	Yellow	0.097	0.229	0.024	121
	Red	0.053	0.207	0.008	89
$CD86_{lat}$*	Yellow	0.122	0.306	0.028	143
	Red	0.200	0.622	0.049	124
TCR_{lat}*	Yellow	0.143	0.605	0.020	107
	Red	0.164	0.351	0.062	92

*Subscript 'lat' denotes cells which were pre-treated with 2.5 μM latrunculin.

Table S4: Protein diffusion coefficients from FCS. Diffusion coefficients for Fab labeled molecules on DO11.10 (murine) T cells from James *et al* are shown for ease of comparison.

		Diffusion Coefficients from FCS
CD28	Green	0.088 ± 0.001
	Red	0.086 ± 0.002
CD86	Green	0.146 ± 0.002
	Red	0.121 ± 0.003
TCR	Green	0.089 ± 0.001
	Red	0.092 ± 0.001

SUPPORTING DISCUSSION

Fluorophore Stability

We note that when compared with Citrine only 70 to 80% of the mCherry tracks were visible (Table S2). Red fluorescent proteins have often been found to have inferior photophysical properties relative to shorter wavelength variants, with recent studies showing complex photophysics (12) and multiple brightness states (13) for mCherry. In addition, a study by Maeder *et al.* using 3xmCherry-tagged molecules in yeast cytoplasm showed that only 50 % of the mCherry molecules in their sample were fluorescent during the course of a measurement (14). This was attributed to the slower maturation time of mCherry, and therefore would be different for our study since the protein turnover rate vs. fluorescent protein maturation rate will be different for receptors in the cell membrane relative to molecules in yeast cytoplasm.

References

1. Naldini, L., U. Blomer, P. Gallay, D. Ory, R. Mulligan *et al.* 1996. In vivo gene delivery and stable transduction of nondividing cells by a lentiviral vector. Science 272:263-267.

2. Axelrod, D. 2008. Total Internal Reflection Fluorescence Microscopy. In Biophysical Tools for Biologists, Vol 2: in Vivo Techniques. Elsevier Academic Press Inc. San Diego. 169-221.

3. Oh, S., L. Schenato, P. Chen, and S. Sastry. 2007. Tracking and coordination of multiple agents using sensor networks: System design, algorithms and experiments. Proceedings of the Ieee 95:234-254.

4. Yoon, J. W., A. Bruckbauer, W. J. Fitzgerald, and D. Klenerman. 2008. Bayesian inference for improved single Molecule fluorescence tracking. Biophysical Journal 94:4932-4947.

5. Crocker, J. C. and D. G. Grier. 1996. Methods of digital video microscopy for colloidal studies. Journal of Colloid and Interface Science 179:298-310.

6. Yoon, J. W. and S. S. Singh. (*in preparation*).

7. Bruckbauer, A., P. James, D. J. Zhou, J. W. Yoon, D. Excell *et al.* 2007. Nanopipette delivery of individual molecules to cellular compartments for single-molecule fluorescence tracking. Biophysical Journal 93:3120-3131.

8. Koyama-Honda, I., K. Ritchie, T. Fujiwara, R. Iino, H. Murakoshi *et al.* 2005. Fluorescence imaging for monitoring the colocalization of two single molecules in living cells. Biophysical Journal 88:2126-2136.

9. Lachmanovich, E., D. E. Shvartsman, Y. Malka, C. Botvin, Y. I. Henis *et al.* 2003. Co-localization analysis of complex formation among membrane proteins by computerized fluorescence microscopy: application to immunofluorescence co-patching studies. Journal of Microscopy-Oxford 212:122-131.

10. James, J. R., S. S. White, R. W. Clarke, A. M. Johansen, P. D. Dunne *et al.* 2007. Single-molecule level analysis of the subunit composition of the T cell receptor on live T cells. Proceedings of the National Academy of Sciences of the United States of America 104:17662-17667.

11. Durand, D. B., J. P. Shaw, M. R. Bush, R. E. Replogle, R. Belagaje *et al.* 1988. Characterization of Antigen Receptor Response Elements within the Interleukin-2 Enhancer. Molecular and Cellular Biology 8:1715-1724.

12. Hendrix, J., C. Flors, P. Dedecker, J. Hofkens, and Y. Engelborghs. 2008. Dark states in monomeric red fluorescent proteins studied by fluorescence correlation and single molecule spectroscopy. Biophysical Journal 94:4103-4113.

13. Wu, B., Y. Chen, and J. D. Muller. 2009. Fluorescence fluctuation spectroscopy of mCherry in living cells. Biophys J 96:2391-2404.

14. Maeder, C. I., M. A. Hink, A. Kinkhabwala, R. Mayr, P. I. H. Bastiaens *et al.* 2007. Spatial regulation of Fus3 MAP kinase activity through a reaction-diffusion mechanism in yeast pheromone signalling. Nature Cell Biology 9:1319-U1226.

Video S1: $TCR_{3xCitrine}$ (*right*) and $TCR_{3x\ mCherry}$ (*left*) raw images on J.RT3 cells. Scalebar is 2 μm.

Video S2: Tracked $CD86_{3xCitrine}$ (blue circles) and $CD86_{3x\ mCherry}$ (red circles) molecules on the surface of Jurkat cells overlaid on the Citrine channel background. Scalebar is 2 μm.

Video S3: Tracked $CD28_{3xCitrine}$ (blue circles) and $CD28_{3xmCherry}$ (red circles) molecules on the surface of J.RT3 cells overlaid on the Citrine channel background. Scalebar is 2 μm.

Video S4: Tracked $TCR_{3xCitrine}$ (blue circles) and $TCR_{3xmCherry}$ (red circles) molecules on the surface of J.RT3 cells overlaid on the Citrine channel background. Scalebar is 2 μm.